Research Article | Vol. 24, No. 15 | 25 Jul 2016 | OPTICS EXPRESS 16752

Optics EXPRESS

Broadband beamsplitter for high intensity laser applications in the infra-red spectral range

TATIANA AMOTCHKINA,[1] HANIEH FATTAHI,[1,2] YURIJ. A. PERVAK,[3] MICHAEL TRUBETSKOV,[1] AND VLADIMIR PERVAK[2,*]

[1]*Max-Planck-Institut für Quantenoptik, Hans-Kopfermann str. 1, 85748 Garching, Germany*
[2]*Ludwig-Maximilians-Universität München, Am Coulombwall 1, 85748 Garching, Germany*
[3]*Taras Schevchenko Kiev National University, Volodymyrska str. 64, 01601, Kyiv, Ukraine*
**Vladimir.Pervak@lmu.de*

Abstract: We report on design, production and characterization of an extremely broadband multilayer beamsplitter, covering wavelength range from 0.67 – 2.6 μm. The group delay dispersion has small oscillations in the above mentioned working range. We used a new algorithm with floating constants allowing us to obtain a smooth and near constant GDD. The optical element based on the beamsplitter is used for dividing a low-energy super-octave spectrum into several sub-spectral regions which are later amplified and coherently combined.

OCIS codes: (310.4165) Multilayer design; (310.6845) Thin film devices and applications; (190.0190) Nonlinear optics; (320.0320) Ultrafast optics.

References and Links

1. S. R. Leone, C. W. McCurdy, J. Burgdörfer, L. S. Cederbaum, Z. Chang, N. Dudovich, J. Feist, C. H. Greene, M. Ivanov, R. Kienberger, U. Keller, M. F. Kling, Z.-H. Loh, T. Pfeifer, A. N. Pfeiffer, R. Santra, K. Schafer, A. Stolow, U. Thumm, and M. J. J. Vrakking, "What will it take to observe processes in "real time"?" Nat. Photonics **8**(3), 162–166 (2014).
2. F. Krausz and M. Ivanov, "Attosecond physics," Rev. Mod. Phys. **81**(1), 163–234 (2009).
3. W. Schweinberger, A. Sommer, E. Bothschafter, J. Li, F. Krausz, R. Kienberger, and M. Schultze, "Waveform-controlled near-single-cycle milli-joule laser pulses generate sub-10 nm extreme ultraviolet continua," Opt. Lett. **37**(17), 3573–3575 (2012).
4. H. Fattahi, H. G. Barros, M. Gorjan, T. Nubbemeyer, B. Alsaif, C. Y. Teisset, M. Schultze, S. Prinz, M. Haefner, M. Ueffing, A. Alismail, L. Vámos, A. Schwarz, O. Pronin, J. Brons, X. T. Geng, G. Arisholm, M. Ciappina, V. S. Yakovlev, D.-E. Kim, A. M. Azzeer, N. Karpowicz, D. Sutter, Z. Major, T. Metzger, and F. Krausz, "Third-generation femtosecond technology," Optica **1**(1), 45–63 (2014).
5. A. Gordon and F. Kärtner, "Scaling of keV HHG photon yield with drive wavelength," Opt. Express **13**(8), 2941–2947 (2005).
6. T. Popmintchev, M.-C. Chen, D. Popmintchev, P. Arpin, S. Brown, S. Alisauskas, G. Andriukaitis, T. Balciunas, O. D. Mücke, A. Pugzlys, A. Baltuska, B. Shim, S. E. Schrauth, A. Gaeta, C. Hernández-García, L. Plaja, A. Becker, A. Jaron-Becker, M. M. Murnane, and H. C. Kapteyn, "Bright coherent ultrahigh harmonics in the keV x-ray regime from mid-infrared femtosecond lasers," Science **336**(6086), 1287–1291 (2012).
7. O. D. Mucke, S. Fang, G. Cirmi, G. M. Rossi, S.-H. Chia, H. Ye, Y. Yang, R. Mainz, C. Manzoni, P. Farinello, G. Cerullo, and F. X. Kartner, "Toward waveform nonlinear optics using multimillijoule sub-cycle waveform synthesizers," IEEE J. Sel. Top. Quantum Electron. **21**(5), 1–12 (2015).
8. H. Hanieh, Fattahi, H. Wang, A. Alismail, and F. Krausz, "Towards high-power, multi-TW light transients," in *Conference on Lasers and Electro-Optics*, OSA Technical Digest (2016) (Optical Society of America, 2016), paper SM1M.6.
9. H. Fattahi, A. Alismail, H. Wang, J. Brons, O. Pronin, T. Buberl, L. Vámos, G. Arisholm, A. M. Azzeer, and F. Krausz, "High-power, 1-ps, all-Yb:YAG thin-disk regenerative amplifier," Opt. Lett. **41**(6), 1126–1129 (2016).
10. A. V. Tikhonravov, M. K. Trubetskov, and G. W. DeBell, "Optical coating design approaches based on the needle optimization technique," Appl. Opt. **46**(5), 704–710 (2007).
11. A. V. Tikhonravov and M. K. Trubetskov, "OptiLayer software," http://www.optilayer.com.
12. M. K. Trubetskov, V. Pervak, and A. V. Tikhonravov, "Phase optimization of dispersive mirrors based on floating constants," Opt. Express **18**(26), 27613–27618 (2010).
13. V. Pervak, A. V. Tikhonravov, M. K. Trubetskov, S. Naumov, F. Krausz, and A. Apolonski, "1.5-octave chirped mirror for pulse compression down to sub-3 fs," Appl. Phys. B **87**(1), 5–12 (2007).
14. D. Ristau, H. Ehlers, T. Gross, and M. Lappschies, "Optical broadband monitoring of conventional and ion processes," Appl. Opt. **45**(7), 1495–1501 (2006).

#267557 http://dx.doi.org/10.1364/OE.24.016752
Journal © 2016 Received 1 Jun 2016; revised 5 Jul 2016; accepted 11 Jul 2016; published 15 Jul 2016

Optics EXPRESS

15. M. Trubetskov, T. Amotchkina, A. Tikhonravov, and V. Pervak, "Reverse engineering of multilayer coatings for ultrafast laser applications," Appl. Opt. **53**(4), A114–A120 (2014).
16. A. N. Tikhonov and V. I. Arsenin, *Solutions of Ill-Posed Problems* (Winston and Sons, 1977).
17. V. Pervak, "Recent development and new ideas in the field of dispersive multilayer optics," Appl. Opt. **50**(9), C55–C61 (2011).
18. V. Pervak, M. K. Trubetskov, and A. V. Tikhonravov, "Robust synthesis of dispersive mirrors," Opt. Express **19**(3), 2371–2380 (2011).
19. L. Gao, F. Lemarchand, and M. Lequime, "Exploitation of multiple incidences spectrometric measurements for thin film reverse engineering," Opt. Express **20**(14), 15734–15751 (2012).
20. I. H. Malitson, "Interspecimen comparison of the refractive index of fused silica," J. Opt. Soc. Am. **55**(10), 1205–1208 (1965).

1. Introduction

To date, advances in attosecond technology is toward generation of isolated attosecond pulses at higher flux and higher photon energies, motivated by several ground-breaking experiments, like imaging electrondynamics in solids at attosecond time-scale, and attosecond-pump attosecond-probe spectroscopy [1,2].

The cutoff energy in high harmonic generation (HHG) can be extended to photon energies above the current state of the art [3], if high-energy single-cycle laser pulses, or sub-cycle light transients in the near-infrared (NIR) or the mid-infrared (MIR) spectral ranges become available [4–6]. Generation of these high-energy waveforms calls for a technique to overcome limitations in energy scalability of the current Ti:Sa laser technology and bandwidth limitations in few-cycle optical parametric chirped pulse amplifiers (OPCPA).

OPCPA-based synthesizers keep promise [4] for generating high-energy pulses with several octave spectral bandwidths. Here a low-energy super-octave spectrum is divided into several sub-spectral regions using a broadband dielectric beamsplitter. Subsequently each spectral region is amplified in OPCPA chains individually and finally the amplified spectra are compressed to their Fourier transform limit by using broadband chirped mirrors and combined coherently with a broadband dielectric beam combiner [4,7].

In this concept design and production of dielectric beamsplitters and beam combiners used to handle such super-octave continua, are immensely complicated and require using effective numerical optimization and accurate deposition tools.

In this paper we report about the design, production and characterization of a sophisticated 96-layers beamsplitter (BS) for dividing a super-octave continuum shown in [8] into two spectral regions which will be amplified by using different harmonics of an Yb:YAG thin disk laser [9] and later coherently combined in the OPCPA-based synthesizer discussed in [4]. To make the synthesizer's geometry simple, the BS is designed to work at the incident angle (AOI) of 45°. In this design the broadband spectrum spanning from 670 nm to 1320 nm, is transmitted, while 1580 nm–2600 nm spectral components are reflected from the BS. Flat group delay dispersion on reflection (GDD) is required by design specifications and the designed BS provides GDD value equal to −235 fs^2. The setup is presented in Fig. 1.

The primary goal of this paper is to demonstrate the feasibility of the complicated multilayer coating. The secondary aim is to point out the challenges in the design-production-characterization chain of complex multilayers in the very broadband spectral range. In Section 2 we consider the theoretical designing of BS and describe produced samples as well as measurement data. In Section 3 we provide optical characterization of the produced samples. Our conclusions are presented in Section 4.

Optics EXPRESS

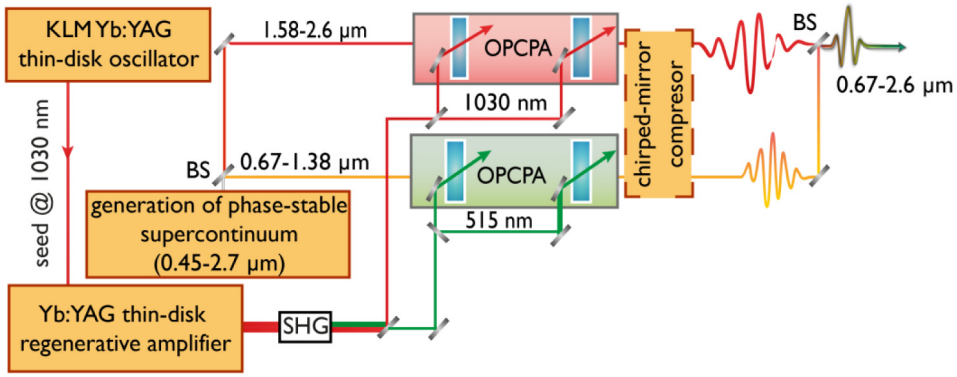

Fig. 1. Set up of a two-channel OPCPA system seeded and pumped by 20 mJ, 1-ps Yb:YAG thin-disk regenerative amplifier [9]. A part of its output is used for generating a phase-stable multi-octave supercontinuum signal, which is split into two channels by using the BS. The two channels are pumped by second-harmonic and the fundamental pulses of the Yb:YAG regenerative amplifier output. Each channel supports few-cycle pulses. By coherently combining the two few-cycle channels using a broadband beam combiner, non-sinusoidal, multi-octave light transients spanning from 0.67–2.6 μm can be generated.

2. Design and production

In our BS we used Nb_2O_5 as high index and SiO_2 as low index materials. We chose two types of the substrates: B260 Glass of 1 mm thickness and Suprasil of 6.35 mm thickness. *Nominal* wavelength dependencies of refractive indices of thin film materials are described by Cauchy formula:

$$n(\lambda) = A_0 + A_1\left(\frac{\lambda_0}{\lambda}\right)^2 + A_2\left(\frac{\lambda_0}{\lambda}\right)^4, \qquad (1)$$

where A_0, A_1, A_2 are dimensionless parameters, $\lambda_0 = 1000\,\text{nm}$, λ is specified in nanometers. For Nb_2O_5 $A_0 = 2.218485$, $A_1 = 0.021827$, $A_2 = 0.004$; for SiO_2 $A_0 = 1.465294$, $A_1 = 0$, $A_2 = 4.7108\cdot10^{-4}$; for B260 Glass $A_0 = 1.51$, $A_1 = 5.254\cdot10^{-3}$, $A_2 = 6.328\cdot10^{-5}$; and for Suprasil $A_0 = 1.443268$, $A_1 = 0.00406$, $A_2 = 6.948\cdot10^{-6}$.

Design of BS was performed with the help of the needle optimization technique incorporated into OptiLayer software [10,11]. A merit function estimating the closeness of the designed spectral characteristics to the target specifications is defined as:

$$MF^2 = \sum_{i=1}^{500}\left(\frac{R_p(\mathbf{X},\lambda_i)}{0.01}\right)^2 + \sum_{j=1}^{500}\left(\frac{R_p(\mathbf{X},\lambda_j)-100}{0.01}\right)^2 + \sum_{j=1}^{500}\left(\frac{GDD_p(\mathbf{X},\lambda_j)-C}{10}\right)^2, \qquad (2)$$

where $\mathbf{X} = \{d_1,...,d_m\}$ is a vector of layer thicknesses, $\{\lambda_i\}$ and $\{\lambda_j\}$ are evenly distributed wavelength points in the spectral ranges from 670 nm to 1320 nm and from 1580 nm to 2600 nm, respectively. Since design specifications required just flat GDD, a constant C is included in Eq. (2), and we used the floating constants approach [12] in order to find a solution with an optimal value of this constant.

Optics EXPRESS

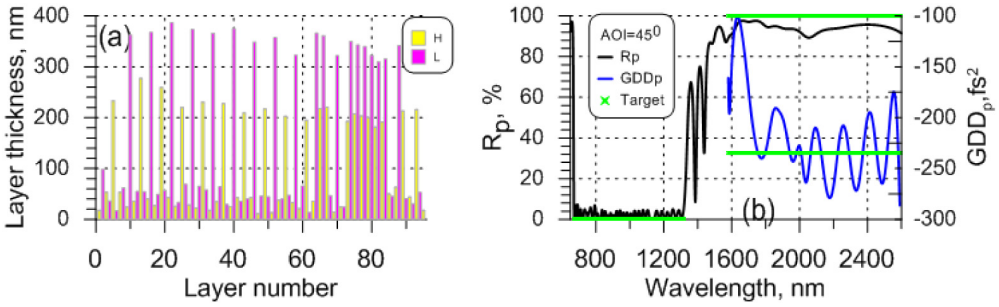

Fig. 2. (a): Refractive index profiles of the BS; (b): Theoretical reflectance and GDD of the BS, green lines indicate target values.

As a result a 96-layer BS was obtained with $C = -235$ fs^2. The BS refractive index profile is shown in Fig. 2(a). Oblique incidence theoretical reflectance R_p and GDD_p (p-polarization) in the spectral ranges of interest are shown in Fig. 2(b). Physical thickness of the obtained design is 13586 nm. The design contains eight layers with thicknesses less than 20 nm. Deposition of such a design is a complicated task requiring not only advanced instrumental tools but also a lot of experience. We produced the designed BS using Leybold Optics magnetron sputtering Helios plant, layer thicknesses were controlled using well-calibrated time monitoring [13]. The plant is equipped with two proprietary TwinMags magnetrons and a plasma source for plasma/ion-assisted reactive middle frequency dual magnetron sputtering. The plant is also equipped with broadband monitoring (BBM) system [14] which was used in a passive mode for data acquisition only. In the deposition run we used the Suprasil substrate for the BS optical element fabrication and the cheaper B260 Glass substrate as a witness sample. As a result, two samples were obtained: BS coating on B260 Glass substrate (sample BS-B260) and BS coating on Suprasil substrate (BS-Suprasil). The transmittance scans (BBM data) were recorded after deposition of each layer of BS-B260 sample.

After the deposition, transmittance data of produced samples were measured by Perkin Elmer Lambda 950 spectrophotometer (PE) in the range from 400 nm to 2500 nm with 0.5 nm wavelength step. Reflectance of the unpolarized light (R_a) and reflectance of the p-polarized light (R_p) at AOI = 45° were taken by the Universal Reflectance Accessory (URA) in the same spectral range. Group delay (GD) and GDD of the BS-Suprasil sample were extracted from white light interferometer (WLI) data. The infra-red detector was used, AOI = 45°, light was p-polarized.

From the experimental data it was found that the reflectance is more than 89% in the spectral range from 1580 nm to 2600 nm and is less than 4% in the range from 670 nm to 1320 nm. The experimental data show that produced BS samples satisfy target specifications and can be used in the OPCPA system shown in Fig. 1.

3. Optical characterization

3.1 Processing of BBM data

In order to improve the coating production in the IR spectral range we perform the characterization of the BS samples. We start with estimating errors in layer thicknesses on the basis of BBM data. We apply the algorithm assuming quasi-random errors in layer thicknesses [11,15]. The algorithm is based on the minimization of *in situ* discrepancy function TDF with respect to relative errors δ_i, $i = 1,...,m$:

Optics EXPRESS

$$TDF^2 = GDF^2 + \frac{\alpha}{m}\sum_{i=1}^{m}\delta_i^2, \quad GDF^2 = \frac{1}{96L}\sum_{i=1}^{96}\sum_{j=1}^{L}\left[T\left(\mathbf{X}_i;\lambda_j\right) - \hat{T}^{(i)}\left(\lambda_j\right)\right]^2, \qquad (3)$$

where $\mathbf{X}_i = \left\{d_1\left(1+\delta_1\right),...,d_i\left(1+d_i\right)\right\}$ is the vector of first i thicknesses of the model coating. The second term in Eq. (3) is responsible for the reliability of the solution taking into account *a priori* information that relative random errors are expected to be quite low. We applied a characterization approach based on the regularization theory of solving ill-posed problems [16]. In Eq. (3) α is a regularization parameter that should be selected in order to provide a balance between data fitting and stability of the solution. In our characterization process we chose $\alpha = 1$.

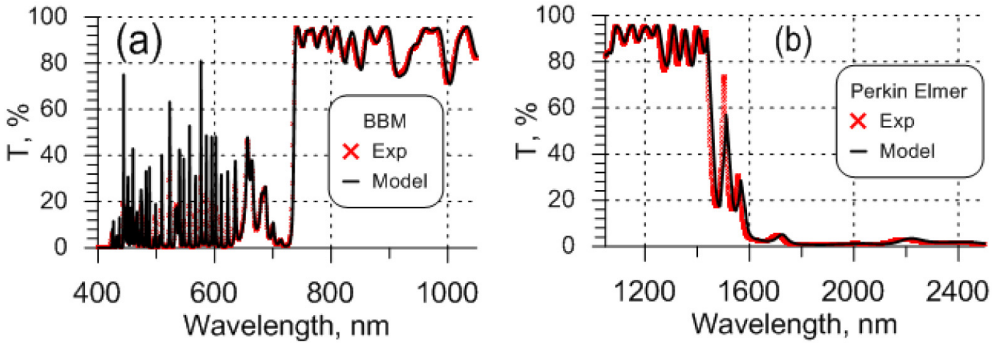

Fig. 3. Comparison of experimental data and transmittance calculated for the model coating (Section 3.1): in the spectral range from 400 nm to 1050 nm where BBM measures (a) and in the IR spectral range from 1050 nm to 2500 nm (b).

Excellent fitting of the BBM data by model data was achieved in the course of characterization process, Fig. 3(a). Estimated errors δ_i do not exceed 2.5% that is in full agreement with expected accuracy of time monitoring [17,18]. Denote $\bar{d}_1 = d_1\left(1+\delta_1\right),...,\bar{d}_m = d_m\left(1+\delta_m\right)$ the thicknesses of the model coating obtained in this way.

3.2 Indices correction

In Fig. 3(b) we compare experimental transmittance in the spectral range from 1050 nm to 2500 nm related to BS-B260 and transmittance curve related to the model coating obtained above. We observe that the correspondence is worse than in the range from 400 to 1050 nm. The deviations can be addressed to inaccuracies in the wavelength dependencies of nominal refractive indices in the IR range. At the next step of the characterization process we correct dispersion curves of Nb_2O_5 and SiO_2. According to Ref [19]. we assume that refractive index of Nb_2O_5 $n_H\left(\lambda\right)$ in the broad range from 400 nm to 2500 nm can be described by the Cauchy formula (see Eq. (1)). In the case of SiO_2 three-parameter Cauchy model may not provide an accurate description of the dispersion behavior in the broad spectral range from 400 nm to 2600 nm. The wavelength dependence of the SiO_2 refractive index having inflection of curve (see Ref [20], Fig. 1) can be only described by more flexible six-parameter Sellmeier model:

$$n^2 = 1 + \frac{B_1\left(\lambda/\lambda_0\right)^2}{\left(\lambda/\lambda_0\right)^2 - B_2} + \frac{B_3\left(\lambda/\lambda_0\right)^2}{\left(\lambda/\lambda_0\right)^2 - B_4} + \frac{B_5\left(\lambda/\lambda_0\right)^2}{\left(\lambda/\lambda_0\right)^2 - B_6}, \qquad (4)$$

where $B_1,...,B_6$ are dimensionless parameters, $\lambda_0 = 1000\,\text{nm}$, λ is specified in nanometers.

We introduce a discrepancy function DF in the standard way:

Optics EXPRESS

$$DF^2 = \frac{1}{L}\sum_{i=1}^{L}\left[T(\mathbf{X};\lambda_i) - \hat{T}(\lambda_i)\right]^2, \quad (5)$$

where $\mathbf{X} = \{\bar{d}_1,...,\bar{d}_m, n_H(\lambda_i), n_L(\lambda_i); \lambda_i\}$ is a vector of model parameters, $n_H(\lambda)$ is specified by Cauchy formula Eq. (1), $n_L(\lambda) = n_{start}(\lambda) + \Delta n_L$, n_{start} is specified by Sellmeier coefficients taken from Ref [20], Δn_L is the refractive index offset, $\hat{T}(\lambda_i)$ are measured normal incidence transmittance data, $\lambda_i = 1050 + 0.5i$, $i = 1,...,2901$. We minimize discrepancy function Eq. (5) with respect to Cauchy parameters A_0, A_1, A_2 and the offset Δn_L. We achieved a good fitting of experimental transmittance by the model data in the range from 1050 nm to 2500 nm. In order to obtain refractive indices in the whole spectral range from 400 nm to 2500 nm we merge nominal indices taken from the range from 400 nm to 1050 nm and estimated indices in the range from 1050 to 2500 nm. As the curve at the junction point is not continuous, we smooth the resulted wavelength dependencies by Cauchy dependence for Nb_2O_5 and Sellmeier dependence for SiO_2. The *corrected* and nominal refractive indices are compared in Fig. 4(a). In this figure one can observe that the deviations between corrected and nominal refractive indices are about 0.02. While Nb_2O_5 refractive index mainly changed by some offset value, SiO_2 refractive index changed qualitatively and the new dependence has an inflection point around 1.2-1.3 μm. It is seen also that the deviations between corrected and nominal refractive indices in the range from 400 nm to 1050 nm are almost negligible. Denote $\bar{n}_H, \bar{n}_L$ the corrected refractive indices of the model coating. In Fig. 4(b) one can observe an excellent correspondence between experimental and model *T*/*R* characteristics in the whole spectral range from 400 nm 2500 nm.

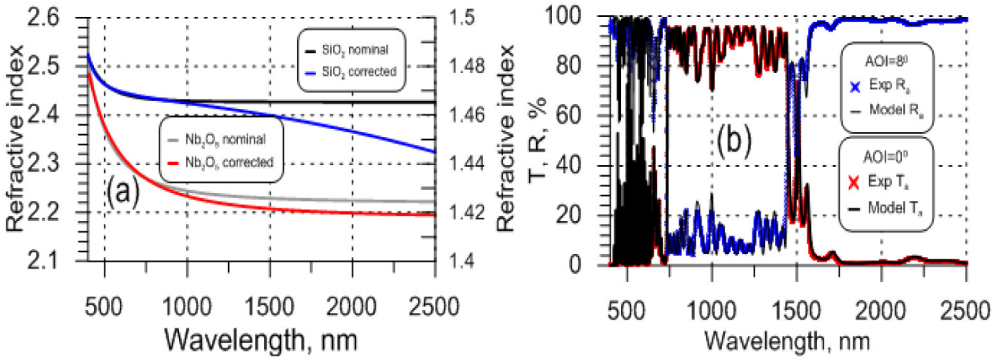

Fig. 4. (a) Comparison of nominal and corrected refractive indices; (b) Comparison of experimental data related to BS-B260 sample and model data calculated for the design BS-B260-2.

3.3 Characterization of BS-Suprasil sample

In the course of the deposition process the deviations between layer thicknesses of the samples placed on the witness and on a calotte position are inevitable. The thickness non-uniformity, however, cannot exceed 1% for Helios machine. Hence, we have to correct thickness errors found for BS-B260 model coating in order to estimate layer errors in BS-Suprasil coating. We assume presence of a systematic shift Δ in layer thicknesses and define a vector of model coating parameters $X = \{\bar{d}_1 + \Delta,..., \bar{d}_m + \Delta; \bar{n}_H, \bar{n}_L; \lambda_j\}$. The systematic shift Δ can be estimated on the basis of the minimization of discrepancy function (Eq. (5)) with experimental data $\hat{T}(\lambda_j)$, $\lambda_j = 400 + j$, $j = 1,...,2101$ related to the BS-Suprasil sample.

Optics EXPRESS

The estimated systematic shift is equal to −0.8%. It is remarkable that the resulted errors in BS-Suprasil coating calculated as $\delta_i + \Delta$ do not exceed 1.7%. We consider a model coating found in this way as a characterization solution for BS-Suprasil sample. In Fig. 5(a), we observe a good correspondence between measured oblique incidence reflectance R_p as well as GD_p with the corresponding model curves. Note that we use GD and GDD data for the verification purposes only, since typically they have lower accuracy and their scales are very different from spectrophotometric data. is For additional verification of the results we compare initial discrepancy function values and discrepancies achieved for final characterization solutions (see Table 1). In this table one can see that in all cases, the final discrepancy function values are decreased in comparison the initial discrepancies. This can be considered as an indication of the reliability of the obtained characterization results.

Table 1. Comparison of initial and final discrepancy function values.

Numerical measure	Sample	Spectral range, nm	Measurement device	Initial value	Final value
GDF (Eq. (3))	BS-B260	400-1050	BBM	8.55	4.26
DF (Eq. (5))	BS-B260	400-2500	PE	6.19	4.45
	BS-Suprasil			8.94	3.42
DF_R (Eq. (5) with R instead of T)	BS-B260		URA	5.87	4.28
	BS-Suprasil			8.48	3.44
DF_{Rp} (Eq. (5) with R_p at AOI = 45° instead of T)	BS-B260			6.56	5.37
	BS-Suprasil			7.23	5.67
GD_p (Eq. (5) with GD_p at AOI = 45° instead of T)	BS-Suprasil	1430-1967	WLI	779	543
GDD_p (Eq. (5) with GDD_p at AOI = 45° instead of T)				740250	525015

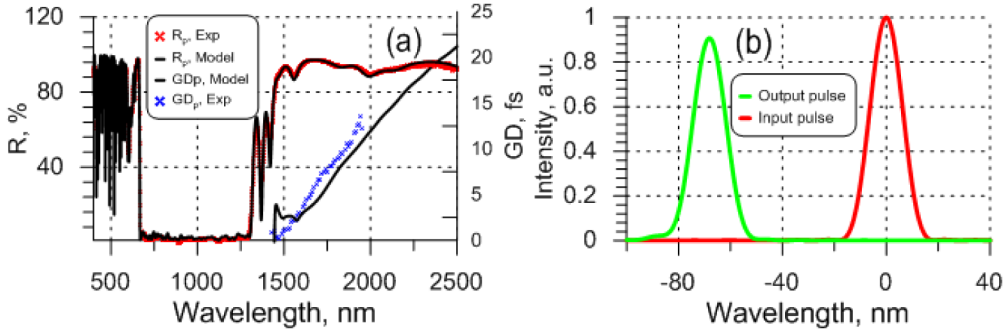

Fig. 5. (a) Comparison of experimental reflectance related to BS-Suprasil sample and model reflectance calculated for the corresponding model coating; (b) Input and output pulse simulations. Output pulse is calculated after reflection from the BS.

In Fig. 5(b) we show the simulated envelopes of the input Fourier-limited pulse and pulse reflected from the BS. It is worse to note that the shape of the reflected pulse is very close to the Fourier-limit one.

4. Conclusions

An outstanding 96-layer beamsplitter for the OPCPA system was designed, produced and characterized. For the first time we have applied floating GDD constant algorithm and were

Optics EXPRESS

able to design smooth and constant GDD in the broadband working range. Good agreement between experimental and theoretical spectral performances demonstrates the applicability of the beamsplitter in the OPCPA systems.

Funding

DFG Cluster of Excellence, "Munich Centre for Advanced Photonics," (http://www.munich-photonics.de); European Union's Horizon 2020 research and innovation programme under the Marie Skłodowska-Curie agreement (657596).